

Cosmology and modified GW propagation from the BNS mass function at third-generation detector networks

Dounia Nanadoumgar-Lacroze ^{a,1,2} Niccolò Muttoni ^{b,c,1}
 Michele Maggiore ^{b,c} Michele Mancarella ^d

^aInstitut de Física d'Altes Energies (IFAE), Barcelona Institute of Science and Technology, E-08193 Barcelona, Spain

^bDépartement de Physique Théorique, Université de Genève, 24 quai Ernest Ansermet, 1211 Genève 4, Switzerland

^cGravitational Wave Science Center (GWSC), Université de Genève, CH-1211 Geneva, Switzerland

^dAix-Marseille Université, Université de Toulon, CNRS, CPT, Marseille, France

E-mail: dnala@ifae.es, niccolo.muttoni@unige.ch, michele.maggiore@unige.ch, mancarella@cpt.univ-mrs.fr

Abstract. We perform forecasts for the Hubble parameter H_0 and for the parameter Ξ_0 that describes modified gravitational-wave propagation, using information from the binary neutron star (BNS) mass function, for Einstein Telescope (ET), taken either in the triangle or in the “2L” configuration, as well as for detector network made by ET together with a 40-km Cosmic Explorer (CE). We restrict ourselves to BNSs with a large signal-to-noise ratio, $\text{SNR} > 50$, which still give $\mathcal{O}(10^3)$ events yr^{-1} , and we perform a full joint cosmology-population Bayesian inference. We find that, for ET in isolation, the two ET configurations perform comparably, yielding uncertainties of 12% and 11% on H_0 for the triangular and 2L designs, respectively, and 18% uncertainty on Ξ_0 in both cases. For networks including ET and CE, we can constrain H_0 and Ξ_0 to precisions of 9% and 6%, respectively. These results should be taken as a very conservative estimate of third-generation detectors’ capabilities as a consequence of the high SNR cut. We project the constraints on the Λ CDM expansion history and find that ET alone (triangular and 2L configurations) achieves its best precision on $H(z)$ at $z = 0.23$ and $z = 0.28$, yielding a 10% and 6% precision, respectively. When CE is added to the network, the precision improves to 4% and 3% at $z = 0.37$ and $z = 0.38$, respectively.

¹Authors to whom correspondence should be addressed.

²This work is part of the doctoral thesis of D.N.L. within the framework of the Doctoral Program in Physics at the Autonomous University of Barcelona.

Contents

1	Introduction	1
2	Modified GW propagation	2
3	Methodology	3
3.1	Population and cosmology hyper-parameters	3
3.2	3G detector networks	7
3.3	BNS event selection	7
4	Results	9
5	Discussion	12

1 Introduction

The possibility of extracting cosmological information from gravitational-wave (GW) observations of compact binary coalescences (CBCs) was recognized long ago [1], and has been the subject of many subsequent studies, e.g. [2–26]. The cosmological usefulness of CBCs is due to the fact that their GW signal allows us to infer the luminosity distance to the source; for this reason these sources are called “standard sirens”, by analogy with the “standard candles” that have a standard (or, rather, standardizable) electromagnetic luminosity. Since the information on cosmology is contained in the relation between luminosity distance and redshift, an independent determination of the redshift to the CBC is also necessary. The GW signal does not carry immediate information on the redshift because of the mass-redshift degeneracy, i.e. the masses m_i of the two initial bodies and the redshift z enter the waveform in the combination $m_i(1+z)$. The simplest scenario that allows us to obtain the source redshift takes place when the GW signal from a CBC has an electromagnetic counterpart (“bright sirens”), so we can identify the host galaxy from the electromagnetic signal. This, however, is now expected to be a rare occurrence, at least at the current second-generation GW detectors LIGO, Virgo and KAGRA. Currently, the only observation of this type is the celebrated binary neutron star (BNS) coalescence GW170817 [27, 28].

In the absence of an electromagnetic counterpart (“dark sirens”), various statistical methods have been developed, such as the combination of a large set of GW events with galaxy catalogs [1, 8, 11, 17, 25, 26, 29–31] or the correlation with features in the mass distribution of black holes and neutron stars (NSs) [9, 10, 19, 21, 22, 32–36] (“spectral sirens”); see [37, 38] for recent reviews. Other possibilities to break the mass-redshift degeneracy include the observation of tidal effects and extraction of the Love number in BNS coalescences (“Love sirens”, [39]).

The perspectives for observations of both bright and dark sirens will improve dramatically at third-generation (3G) detectors, such as the Einstein Telescope (ET) [40–42] and Cosmic Explorer (CE) [43–45]. In particular, 3G detectors are expected to observe $\mathcal{O}(10^5)$ binary black hole (BBH) and BNS events per year [46, 47] and, with such a large statistical sample, dark sirens techniques can become very effective. Another scenario that opens up

for 3G detectors is the possibility of localizing a GW event sufficiently well that in the localization volume there is just one galaxy [48, 49]; for 3G detectors there can be a handful of such events per year, see figure 2.28 of [47]. We refer the reader to Section 2.3.1 of [47] for a review of the various dark sirens methods, and their applicability to 3G detectors. It is important to stress that the inference of the cosmological parameters with these statistical techniques is intertwined with the inference of the astrophysical population parameters, such as the redshift and mass distribution of the sources [25, 30, 33, 50–52] (or, for the Love sirens method, the parameters describing the NS equation of state).

In this paper we discuss how to extract cosmological parameters, and especially those that describe modified GW propagation (due to modifications of gravity at cosmological scales), using the BNS mass function. The idea of using the BNS mass function for extracting cosmological information was proposed in [2, 9, 10] in the context of the determination of H_0 within Λ CDM. In [19] it was discussed how to apply this idea to modified GW propagation, showing that the method can be quite promising for testing modifications of gravity. Here we will present a quantitative discussion of the perspectives at 3G detector networks, performing a joint cosmology and population Bayesian analysis. The paper is organized as follows. In section 2, we briefly review modified GW propagation and the current limits on the main parameter, Ξ_0 , that describes it phenomenologically. In section 3, we present the basic set-up of our analysis, i.e. the 3G detector networks used, the BNS population model, and the technical tools used in this study. In section 4, we present our results before concluding in section 5.

2 Modified GW propagation

The phenomenon of modified GW propagation refers to the fact that, in theories where General Relativity (GR) is modified at cosmological scales, the propagation of GWs across cosmological distances is, in general, also modified. In particular, in modified gravity theories that do not affect the speed of GWs (which, after the observation of GW170817, is now excluded at a level of about a part in 10^{15} [28]), the evolution of tensor perturbations over a Friedmann-Lemaître-Robertson-Walker (FLRW) background is governed by the equation¹

$$\tilde{h}_A'' + 2\mathcal{H}[1 - \delta(\eta)]\tilde{h}_A' + c^2k^2\tilde{h}_A = 0, \quad (2.1)$$

where $\delta(\eta)$ is a function that encodes the modifications from GR, so that GR is recovered for $\delta(\eta) = 0$. This behavior has been found in many explicit modified gravity models [53–63]. A consequence of this modification is that the amplitude of the GW generated by a CBC is no longer proportional to the inverse of the luminosity distance $d_L(z)$ of the source (which, in this context, we denote by $d_L^{\text{em}}(z)$, since this is the quantity that would be measured from an electromagnetic counterpart). Rather, it is proportional to the inverse of a “GW luminosity distance” $d_L^{\text{gw}}(z)$ [57], related to $d_L^{\text{em}}(z)$ by [57, 59]

$$\frac{d_L^{\text{gw}}(z)}{d_L^{\text{em}}(z)} = \Xi(z), \quad (2.2)$$

where

$$\Xi(z) = \exp \left\{ - \int_0^z \frac{dz'}{1+z'} \delta(z') \right\}, \quad (2.3)$$

¹We use standard notation: $\tilde{h}_A(\eta, \mathbf{k})$ is the Fourier-transformed GW amplitude, $A = +, \times$ labels the two GW polarizations, the prime denotes the derivative with respect to cosmic time η , defined by $d\eta = dt/a(t)$, $a(\eta)$ is the scale factor, and $\mathcal{H} = a'/a$.

and the function δ that appears in eq. (2.1) has now been written as a function of redshift. A full reconstruction of the function $\Xi(z)$ from future GW observations is a challenging task. Although partial reconstructions are possible, for instance using Gaussian process techniques [64], it is often more practical, as in the case of the dark energy (DE) equation of state, to work within a parametrized framework. A convenient parametrization is given by [59]

$$\Xi(z) = \Xi_0 + \frac{1 - \Xi_0}{(1+z)^n}, \quad (2.4)$$

and is characterized by two parameters (Ξ_0, n) . This form yields a smooth power-law interpolation in the scale factor $a = 1/(1+z)$, connecting the present-day limit $d_L^{\text{gw}}/d_L^{\text{em}} = 1$ at $z = 0$ (corresponding to the absence of propagation effects) to a constant value at high redshift. The latter behavior is well motivated, since in typical modified gravity scenarios departures from GR occur only in the recent cosmological past. Consequently, $\delta(z)$ vanishes at large redshift and the integral in eq. (2.3) approaches a constant. The GR limit is recovered for $\Xi_0 = 1$, independently of the value of n . This simple parametrization has been shown to provide an excellent description covering a broad range of well-studied modified gravity models such as $f(R)$ gravity, [65, 66], Jordan-Brans-Dicke theory [67], Galileon theories [68, 69], and non-local gravity [62, 70, 71]; see [63] for detailed discussion. It should be observed that, in the parametrization (2.4), GR is recovered not only for $\Xi_0 = 1$ (and arbitrary n) but also for $n = 0$ (and arbitrary Ξ_0). To get rid of this potential ambiguity, when performing a Bayesian analysis we will set a prior $n \geq n_{\text{min}}$, with n_{min} strictly positive, see section 3.

Several limits on modified GW propagation have already been obtained from current GW observations (see section 2.3.2.2 of [47] for a recent overview). In general, significant limits on n in eq. (2.4) cannot yet be obtained from current data; however, interesting limits on deviations from GR, as quantified by the deviation of Ξ_0 from the GR value $\Xi_0 = 1$, have already been found. The most recent and stringent result, $\Xi_0 = 1.0^{+0.4}_{-0.2}$ (with a narrow prior on H_0 , and 68% c.l.), was obtained by the LVK Collaboration [72] using the GWTC-4.0 catalog of GW events [73, 74] and combining them with both galaxy catalogs and the mass distribution of CBCs. Related analyses based on earlier GW catalogs and different modeling assumptions were presented in [17, 21, 23, 51, 75–78].

3 Methodology

3.1 Population and cosmology hyper-parameters

To perform a joint inference on the population and cosmological parameters we use a hierarchical Bayesian approach. This technique is by now standard in this context, and we refer the reader to the original papers and reviews [79–83] for general discussion of the method. We adopt the Bayesian framework developed in ICAROGW, which models GW detections as a noisy, inhomogeneous and incomplete Poisson process [31]. The hierarchical likelihood used to infer hyper-parameters Λ is defined as

$$\mathcal{L}(\{x\}|\Lambda) \propto \prod_{i=1}^{N_{\text{obs}}} \frac{\int \mathcal{L}(x_i|\theta, \Lambda) \frac{dN}{dt d\theta}(\Lambda) dt d\theta}{\int p_{\text{det}}(\theta, \Lambda) \frac{dN}{dt d\theta}(\Lambda) dt d\theta}, \quad (3.1)$$

where N_{obs} is the number of detections, each described by a set of parameters θ , in a dataset $\{x\}$; $\mathcal{L}(x_i|\theta, \Lambda)$ are the individual likelihood terms, $\frac{dN}{dt d\theta}(\Lambda)$ is the event production rate, and

$p_{\text{det}}(\theta, \Lambda)$ accounts for the selection effects. Integrals are estimated relying on Monte Carlo integration. More details can be found in [31].

We apply this method to a set of BNS observations, using as prior information the mass and redshift distributions. We do not combine it with information from the galaxy catalog method (as in [72]), since our aim here is to assess the constraining power of the method based on the BNS mass function prior. The two crucial ingredients of the method based on the mass and redshift information are the redshift prior and the mass prior. For the former, we take a Madau-Dickinson parametrization [84, 85],

$$\psi(z) \propto \frac{(1+z)^\gamma}{1 + \left(\frac{1+z}{1+z_p}\right)^{\gamma+\kappa}}, \quad (3.2)$$

convoluted by a log-flat time-delay distribution to keep into account binary evolution (see analogous methodologies in refs. [49, 86, 87]). The detector-frame BNS redshift distribution then reads

$$R(z | \Lambda_z) \propto \psi(z) \frac{1}{(1+z)} \frac{dV}{dz}, \quad (3.3)$$

where dV/dz is the differential comoving volume element and the $(1+z)$ factor at the denominator accounts for the source-frame to detector-frame time interval transformation. The normalization factor of eq.(3.3) is the local BNS merger rate R_0 , while the redshift z_p is the peak of the star formation rate (which is in the range $z_p \sim 1.5 - 3$), and γ and κ are constants, defined so that this functional form interpolates between a power-like behavior $R(z) \propto (1+z)^\gamma$ for redshifts well below z_p , and $R(z) \propto (1+z)^{-\kappa}$ at $z \gg z_p$.

For the mass prior on the two BNS masses m_1 and m_2 , we assume a joint flat distribution between m_{min} and m_{max} defined as

$$p(m_1, m_2) dm_1 dm_2 = \frac{1}{\mathcal{N}} dm_1 dm_2, \quad (3.4)$$

where the normalization factor \mathcal{N} is determined by requiring that $m_2 < m_1$. Specifically

$$\begin{aligned} \mathcal{N} &= \int_{m_{\text{min}}}^{m_{\text{max}}} dm_1 \int_{m_{\text{min}}}^{m_1} dm_2 \\ &= \int_{m_{\text{min}}}^{m_{\text{max}}} (m_1 - m_{\text{min}}) dm_1 \\ &= \frac{1}{2} (m_{\text{max}} - m_{\text{min}})^2. \end{aligned} \quad (3.5)$$

The population hyper-parameters, i.e. the parameters on which we will perform the inference, are therefore

$$\Lambda_{\text{pop}} = \{\gamma, \kappa, z_p, m_{\text{min}}, m_{\text{max}}\}. \quad (3.6)$$

For cosmological inference, we consider two different scenarios. First, we consider the standard (spatially flat) Λ CDM model. The expression of the luminosity distance as a function of redshift is then given by the usual expression

$$d_L(z) = \frac{c}{H_0} (1+z) \int_0^z \frac{d\tilde{z}}{\sqrt{\Omega_M(1+\tilde{z})^3 + \Omega_R(1+\tilde{z})^4 + \Omega_\Lambda}}, \quad (3.7)$$

where Ω_M is the present matter fraction, Ω_R that of radiation (which we have written for completeness, but is completely negligible at the redshifts where astrophysical compact binaries merge), and Ω_Λ is the energy density associated to a cosmological constant; for a spatially flat cosmology, $\Omega_M + \Omega_R + \Omega_\Lambda = 1$. In this case, the cosmological hyper-parameters are

$$\Lambda_{\text{cosmo}} = \{H_0, \Omega_M\}. \quad (3.8)$$

We then consider the modified gravity scenario. In this case, we fix H_0 and Ω_M to their Planck 2018 values (this is essentially equivalent to the narrow H_0 prior used in [72]) and, in general, the DE density becomes a function of redshift, $\Omega_{\text{DE}}(z)$; furthermore, the quantity extracted from the GW observation is the GW luminosity distance, related to the standard electromagnetic luminosity distance by eqs. (2.2) and (2.4), so the relation between the quantity d_L^{gw} measured by GW observations and the redshift of the source is

$$d_L^{\text{gw}}(z) = \Xi(z) \frac{c}{H_0} (1+z) \int_0^z \frac{d\tilde{z}}{\sqrt{\Omega_M(1+\tilde{z})^3 + \Omega_R(1+\tilde{z})^4 + \Omega_{\text{DE}}(\tilde{z})}}. \quad (3.9)$$

For $\Xi(z)$ we adopt the parametrization (2.4). For $\Omega_{\text{DE}}(z)$ a standard choice is the CPL parametrization [88, 89]

$$\Omega_{\text{DE}}(z) = \Omega_{\text{DE}} \exp \left\{ 3 \int_0^z \frac{d\tilde{z}}{1+\tilde{z}} [1 + w_{\text{DE}}(\tilde{z})] \right\}, \quad (3.10)$$

where $\Omega_{\text{DE}} = \Omega_{\text{DE}}(z=0)$ and

$$w_{\text{DE}}(z) = w_0 + \frac{z}{1+z} w_a. \quad (3.11)$$

With H_0 and Ω_M fixed (and Ω_R fixed but in any case negligible), the cosmological hyper-parameters are therefore

$$\Lambda_{\text{cosmo}} = \{\Xi_0, n, w_0, w_a\}. \quad (3.12)$$

It should be observed, however, that (in a generic modified gravity theory, where these parameters are independent from those characterizing background evolution and scalar perturbations) the determination of Ξ_0 and n can only be obtained with GW observations, while $\{w_0, w_a\}$, as well as $\{H_0, \Omega_M\}$, can be obtained from electromagnetic observations. In the following, we will assume that, by the time ET operates, narrow priors will be available on all quantities that can be determined electromagnetically, and we will use GW observation to infer Ξ_0 and n . Therefore, among the cosmological parameters, we will perform the inference only on them, and our set of cosmological parameters for the modified gravity case will be

$$\Lambda_{\text{cosmo}} = \{\Xi_0, n\}. \quad (3.13)$$

In particular, the cosmological parameters H_0 and Ω_M are determined by a large number of electromagnetic observations, so narrow priors are already available on them (and are expected to be even more stringent when 3G detectors will operate, in particular for H_0); of course, performing an inference on H_0, Ω_M from GW alone is interesting to see how much information GW observations can add to electromagnetic observations (in particular for H_0 , in view of the Hubble tension, see [90] for a recent discussion). In contrast, performing an inference on $\{\Xi_0, n\}$ assuming that all we know on H_0 and Ω_M comes from the BNS mass function itself is not very meaningful, and would artificially worsen the forecasts on $\{\Xi_0, n\}$.

Parameter	Prior range (Uniform)	Fiducial value
H_0	[10, 200] km s ⁻¹ Mpc ⁻¹	67.66 km s ⁻¹ Mpc ⁻¹
Ω_M	[0.05, 0.99]	0.30966
Ξ_0	[0.5, 2]	1
n	[0.3, 5]	1.91
γ	[0, 12]	1.42
κ	[0, 6]	4.62
z_p	[0, 4]	1.84
m_{\min}	[0.1, 5] M_\odot	1 M_\odot
m_{\max}	[0.1, 5] M_\odot	2.5 M_\odot

Table 1. Prior distributions and fiducial values adopted for the parameters reported in the leftmost column.

The set of priors used on the population and cosmological data is shown in the middle column of table 1. It is worth commenting on the prior on n in the modified gravity case. As we have mentioned, the parametrization (2.4) reduces to GR both for $\Xi_0 = 1$ (and arbitrary n) and for $n = 0$ (and arbitrary Ξ_0). If we only recovered GR for $\Xi_0 = 1$ and arbitrary n , the fact that GR corresponds to a line in parameter space, rather than to a point, by itself would not be a problem; the consistency with GR, or the deviations from it, would simply be quantified using the posterior for Ξ_0 marginalized over n . However, the existence of the GR line $n = 0$ for arbitrary Ξ_0 complicates the picture. Furthermore, this can create numerical problems in the numerical exploration of the parameter space, since for n very close to zero the Markov Chain Monte Carlo (MCMC) is led to explore arbitrarily large values of Ξ_0 , resulting in unphysical tails in the posterior for Ξ_0 ; similarly, for Ξ_0 close to one, the MCMC could explore arbitrary values of n . These problems are cured with a physically-motivated choice of prior for n . The parametrization (2.4) has been compared with the explicit behavior of $d_L^{\text{gw}}(z)/d_L^{\text{em}}(z)$ for a broad range of modified gravity models. Actually, it was first inspired by non-local gravity, where it turns out that $n \sim 2 - 2.5$ (with precise values depending on the initial conditions of the model) in both the model of ref. [70], see [61], and in the model of ref. [71], see [59]. The predictions for n in a broad class of modified gravity models are shown in table 1 of [63]. While they generically depend on some free parameters, one sees from this table that typical values are not expected to be very close to zero (nor very large). For instance, in $f(R)$ gravity, adopting the functional form for $f(R)$ proposed by Hu and Sawicki [66], one gets (setting $\Omega_M = 0.3$) $n \simeq 0.3(\tilde{n} + 1)$, where \tilde{n} is a positive quantity, so $n \gtrsim 0.3$; in “designer $f(R)$ gravity” [91], setting again $\Omega_M = 0.3$, one finds $n \simeq 2.3$; as another example, in models where the function $\delta(z)$ in eq. (2.1) follows the dark-energy density, $\delta(z) = \delta_0 \Omega_\Lambda(z)/\Omega_\Lambda$, one finds $n = 3\Omega_\Lambda/\log(1/\Omega_M) \simeq 1.7$; see [63]. The bottomline is that, in typical models, n is a number of order one, neither very close to zero nor very large. When performing a Bayesian analysis, we will then set a prior $n \in [n_{\min}, n_{\max}]$; we choose in particular $n_{\min} = 0.3$ and $n_{\max} = 5$. We find that the precise choice of n_{\max} is not very important. In contrast, setting a prior $n \geq n_{\min}$ with n_{\min} strictly positive is important, otherwise we found that, in posterior of Ξ_0 , large tails can be generated in the high- Ξ_0 region; in these cases we found that, even if the peak of the Ξ_0 posterior lies over the fiducial value, the high- Ξ_0 tail introduces a significant offset in the median value, see appendix 5 for details. We found that the value $n_{\min} = 0.3$ is a good compromise between not restricting too much the parameter space, and ensuring

numerical stability, and that the results do not change much taking a larger value of n_{\min} (while the error on Ξ_0 that we will present below might increase by a factor of order 2-3, when moving from $n_{\min} = 0.3$ down to $n_{\min} = 0$).

3.2 3G detector networks

We consider ET both in isolation and in a network with CE. For ET we consider the two configurations currently under consideration by the ET Collaboration, namely a triangle with 10-km arms (denoted “ET- Δ ”), and a configuration with two L-shaped detectors, each with 15 km arms, in two different sites (denoted “ET-2L”).

In the ET-2L setting, for definiteness the two L-shaped detectors will taken to be in the two candidate sites in Sardinia and in the Meuse-Rhine region, but no significant difference will appear with one L-shaped detector in Sardinia and the other in the candidate site near Kamenz, in the Lusatia region in Saxony. Indeed the great circle chord distance between the Sardinia site and the site in the Meuse-Rhine is 1165.0 km, while that between the Sardinia site and Kamenz is 1247.3 km, so the two distances are quite comparable, with the Sardinia-Kamenz distance larger by about 7%. In contrast, the great circle chord distance between Kamenz and the site in Meuse-Rhine is 575.4 km, significantly smaller, so all results concerning in particular angular localization would worsen significantly. In the ET-2L configuration, the two L-shaped detectors are taken to be oriented at 45° to each other, where the relative orientation between two L-shaped detectors is defined with reference to the great circle that connects them [92, 93], similarly to what done in ref. [46], where a detailed comparison of the science output of these configurations was presented.²

The sensitivity curve used for ET and for CE, as well as the location of the CE-40km detector, are also the same as in ref. [46].

3.3 BNS event selection

We consider a BNS population described by the source parameters set

$$\boldsymbol{\theta} = \{\mathcal{M}, \eta, d_L, \chi_{1z}, \chi_{2z}, \theta, \phi, \iota, \psi, \Phi_{\text{coal}}, t_{\text{coal}}\}, \quad (3.14)$$

where \mathcal{M} is the chirp mass, η is the symmetric mass ratio, d_L is the luminosity distance, χ_{1z} and χ_{2z} are the dimensionless z -oriented spin components of the two compact objects, θ and ϕ are the colatitude and longitude, ι and ψ are the inclination and polarization angle, while Φ_{coal} and t_{coal} are the coalescence phase and time. For generating the BNS population, angles are generated assuming isotropy and uniformity. Distance and mass parameters are extracted from the redshift and individual mass distributions given in eqs. (3.3) and (3.4) with the appropriate transformations. The value of the fiducial parameters are shown in the rightmost column of table 1. In particular, the Madau-Dickinson profile parameters γ , κ and z_p are taken from ref. [86], while R_0 , m_{\min} and m_{\max} are chosen from the SIMPLE UNIFORM BNS model³ reported in ref. [94]. In the injected population, we assume for simplicity the spin parameters to be identically zero, but we include them in the source parameter reconstruction

²Actually, in ref. [46] a small offset from 45° was used in order not to send to zero the sensitivity to stochastic backgrounds (such small offset has little or no impact on parameter estimation for CBCs). Here we are only interested in CBCs, so we will not add such a small offset.

³The BNS local merger rate is mass function dependent and ranges from $\mathcal{O}(10)$ to $\mathcal{O}(10^2)$. Following ref. [94], results from the FULLPOP-4.0 model feature a broad interval ($7.6 - 250 \text{ Gpc}^{-3} \text{ yr}^{-1}$), while SIMPLE UNIFORM yields tighter bounds ($13 - 170 \text{ Gpc}^{-3} \text{ yr}^{-1}$). We choose to use the midpoint value of the latter range, as it matches our mass distribution assumptions and falls safely within both intervals.

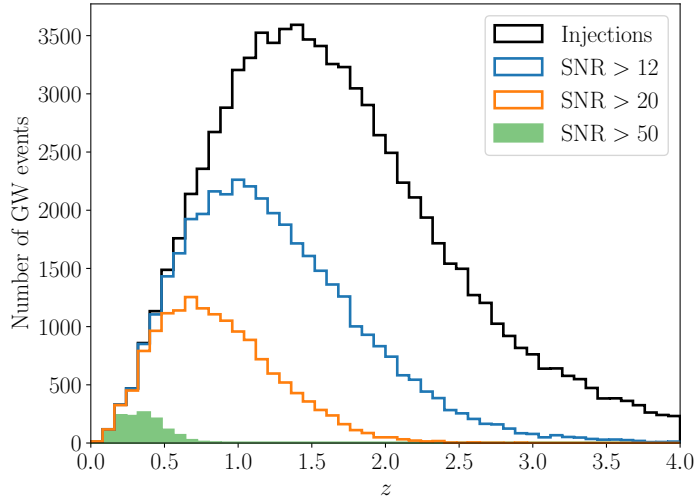


Figure 1. The distribution in redshift of the observed BNSs, for different cuts on the network SNR, for a network ET-2L+CE-40km. The black curve is the full injected BNS population, while the colored curves show the distribution of the events recovered with a given SNR threshold. In particular, the green-filled histogram represents the employed dataset.

of the signals. With these settings we obtain a total of 86049 events per year. Each event is then projected, assuming the IMRPHENOMD waveform model [95], over the detectors’ sensitivity curves, from $f_{\min} = 2$ Hz to from $f_{\max} = 2048$ Hz. We adopt a 100% duty factor throughout the year and, due to the typical length of BNS signals at 3G detectors ($\mathcal{O}(1)$ day), the Earth’s rotation is included. Fisher matrices are then computed for the whole set of source parameters $\boldsymbol{\theta}$, resulting in a 11×11 matrix for each event. We recover posterior samples by the direct sampling of the high-SNR limit of the single-event posterior, defined as

$$p(\boldsymbol{\theta})d\boldsymbol{\theta} \propto \exp\left(-\frac{1}{2}\Delta\theta_i\Gamma_{ij}\Delta\theta_j\right)d\boldsymbol{\theta}, \quad (3.15)$$

where Γ represents the Fisher matrix. To avoid ill-conditioned results we exclude from this procedure all the events for which

$$\delta_{\text{inv}} = \max_{i,j} \left| (\Gamma\Sigma)_{ij} - \mathbb{I}_{ij} \right| > 5 \times 10^{-2}, \quad (3.16)$$

where $\Sigma = \Gamma^{-1}$ and \mathbb{I} is the identity matrix. The catalog generation relies on the python package MGCOSMOPOP [21], while the whole Fisher-matrix-related approach mentioned above is performed through the python library GWFAST [96], to which we refer the reader for more details.

We decided to focus only on the BNSs for which the network signal-to-noise ratio (SNR) is relatively high, setting a threshold at $\text{SNR} \geq 50$. This still gives $\mathcal{O}(10^3)$ BNSs/yr for a 3G network involving ET and CE, and $\mathcal{O}(10^2)$ BNSs/yr events for ET alone; this is still a significant sample, that allows us to perform a meaningful dark siren study. For a full 3G network with both ET and CE, the size of the sample could be increased by a factor about ~ 10 (~ 30) lowering the SNR to 20 (12). Analogously, for an ET-only observatory, the size would increase by a factor of about ~ 13 (~ 50). However, we found that this introduces biases in the reconstruction of the injected values of the hyper-parameters. In particular,

the poorer parameter estimation associated with low-SNR events can bias the exploration of parameter space toward incorrect regions, as the Fisher matrix approximation becomes increasingly unreliable in the low-SNR regime. Furthermore, our simulation does not take into account the effect on the parameter estimation due to the specific noise realization. While high-SNR events are not affected by this, a lower threshold makes the noise contribution less negligible and should be therefore taken into account properly. Thus, to be on the safe side, we eventually restricted our analysis to the BNSs with $\text{SNR} \geq 50$. This means that we are selecting BNSs at relatively low redshift. Figure 1 shows the distribution in redshift of the observed BNSs, for different cuts on the network SNR, for a network ET-2L+CE-40km; we see that all BNSs that pass this cut are at $z < 0.8$. On the one hand, the BNSs that do not pass this cut will have in general a worse parameter reconstruction, because they have a lower SNR, so in this sense one might think that they would (individually) contribute less to the determination of the cosmological parameters; on the other hand, modified GW propagation is a phenomenon that grows with redshift, and vanishes as $z \rightarrow 0$, so the most distant objects are also those where the effect is more significant. Therefore, it is clear that restricting ourselves to BNSs with $\text{SNR} \geq 50$ will provide a conservative — and possibly a very conservative — forecast on the parameter Ξ_0 .

4 Results

In this section we present the results obtained for the following networks: ET- Δ , ET-2L, ET- Δ +CE-40km and ET-2L+CE-40km. The $\text{SNR} = 50$ cut and the Fisher matrix inversion check leave, respectively, 163, 378, 962 and 1237 GW events to be employed in the hyper-parameter inference. We explore the parameter space using the ICAROGW wrapper of the nested sampling algorithm ULTRANEST [97]. The sampler is run with a standard evidence-based convergence criterion, controlled by the parameter `remainder_fraction`. We adopt `remainder_fraction` = 0.01, such that the sampling is terminated once the estimated remaining contribution to the Bayesian evidence from the unexplored prior volume falls below 1% of the evidence accumulated up to that point. This ensures that the evidence estimate has converged to the percent level.

Network	H_0	Ω_M	γ	κ	z_p	m_{\min}	m_{\max}	z_{best}	$H(z_{\text{best}})$
ET- Δ	0.12	1.02	0.91	0.45	0.77	0.017	0.016	0.23	0.10
ET-2L	0.11	0.87	0.93	0.45	0.80	0.012	0.014	0.28	0.06
ET- Δ +CE-40km	0.09	0.47	0.28	0.47	0.58	0.010	0.010	0.37	0.04
ET-2L+CE-40km	0.09	0.48	0.26	0.47	0.64	0.010	0.011	0.38	0.03

Table 2. Relative precision (as defined in footnote 4) achieved for the cosmology and population hyper-parameters in Λ CDM cosmology, for the different network configurations. The columns labeled z_{best} and $H(z_{\text{best}})$ refer respectively to the redshift at which $H(z)$ is best constrained and the relative precision on $H(z)$.

Tables 2 and 3 summarize the relative precision with which parameters are measured, for the cases of Λ CDM and of modified gravity, respectively.⁴ Similarly, figure 2 shows the

⁴Given that the posteriors are in general not symmetric, we computed the relative precision on each parameter in tables 2 and 3 as $(q_{84} - q_{16})/(2\mu)$, where q_n is the n -th quantile of the marginalized distributions and μ is the relevant fiducial value. This gives the 68% c.l. and reduces to the standard 1σ error for a

Network	Ξ_0	n	γ	κ	z_p	m_{\min}	m_{\max}
ET- Δ	0.18	0.84	1.07	0.44	0.76	0.013	0.010
ET-2L	0.18	0.77	1.00	0.44	0.80	0.008	0.008
ET- Δ +CE-40km	0.06	0.87	0.30	0.46	0.57	0.005	0.005
ET-2L+CE-40km	0.06	0.83	0.30	0.47	0.62	0.005	0.004

Table 3. Relative precision (as defined in footnote 4) achieved for the cosmology and population hyper-parameters in modified gravity, for the different network configurations. H_0 and Ω_M are now fixed to their fiducial values.

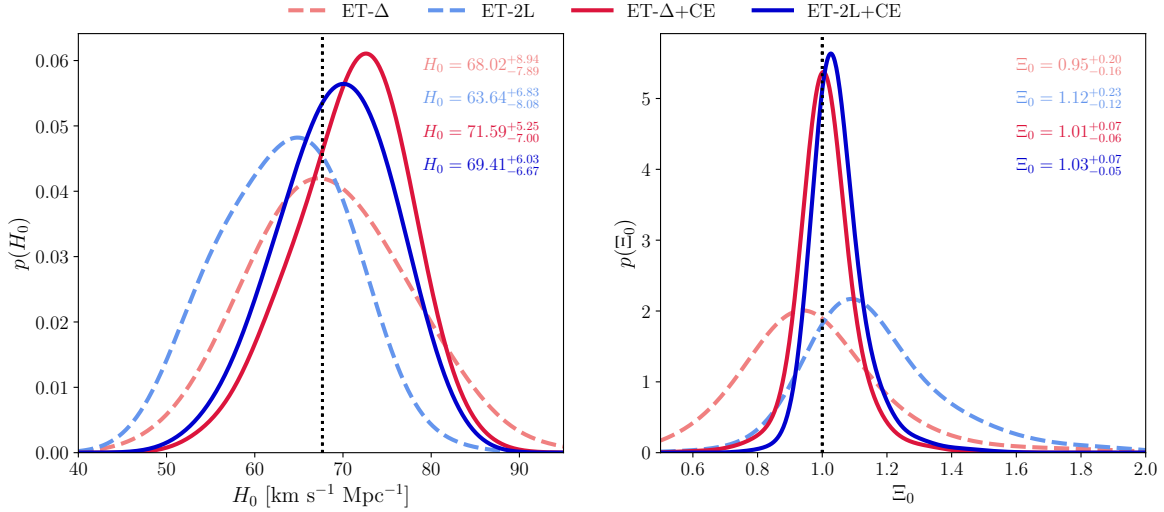


Figure 2. Posterior distributions for H_0 (left) and Ξ_0 (right) marginalized over the other hyper-parameters for the four networks considered. The black dotted line shows the fiducial values as referenced in table 1. The posteriors are smoothed using a kernel distribution estimate.

posterior distributions for H_0 and Ξ_0 , marginalized over the rest of the parameters, for all network configurations. A first remark is that both 3G networks perform similarly, regardless of the different number of events. Regarding Ξ_0 , there is a significant improvement when CE is included in the network, whereas the change of ET configuration has no impact on the precision. This can be explained by the fact that the effect of modified gravity, as described by eq. (2.4), goes to zero as $z \rightarrow 0$ and grows monotonically with redshift, and the large redshift range is more extensively probed by adding a CE detector.

Finally, figure 3 shows the results on the hyper-parameters for ET alone (triangle and 2L) and Λ CDM or modified gravity, while figure 4 shows the analogous results when ET is in a network with CE. The constraints on H_0 are driven by its strong correlation with Ω_M and the mass model parameters m_{\min} and m_{\max} , as expected from the mass-redshift degeneracy. Regarding the redshift evolution parameters, while γ is well recovered owing to good coverage of our population in the redshift region $z < z_p$, κ and z_p are not well constrained due to a lack of events passing our cuts at redshifts above the Madau-Dickinson peak. For this reason, κ and z_p are marginalized over in figures 3 and 4.

symmetric posterior.

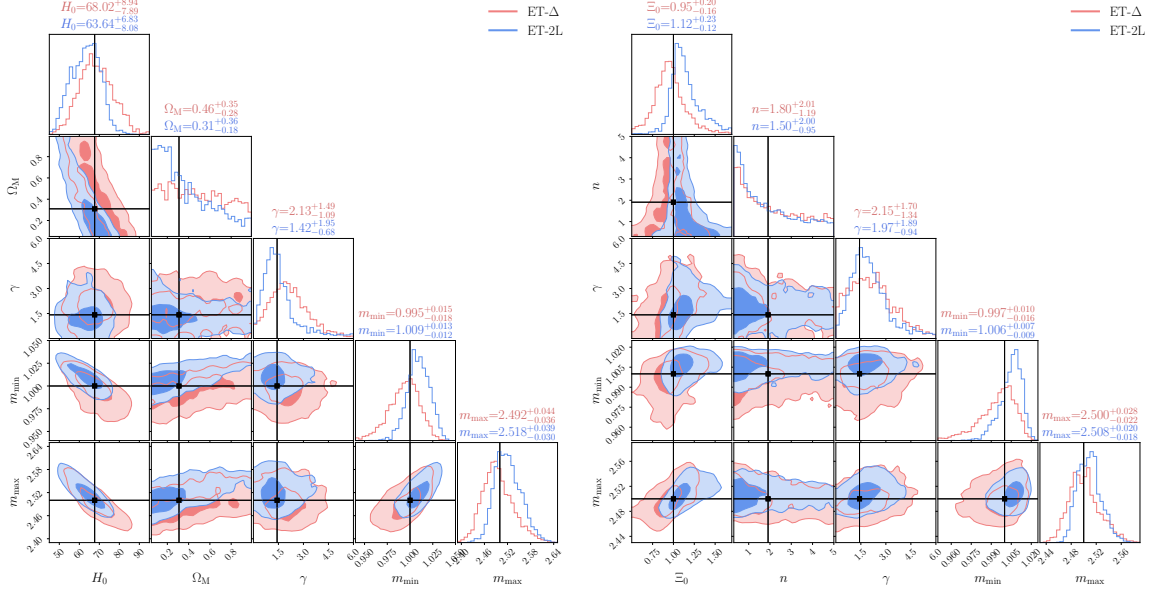


Figure 3. Posterior distributions of the parameters shown at the bottom for the ET- Δ and ET-2L network configurations. Contour shades represent, from dark to light, 1σ and 2σ credible regions. The black lines refer to the fiducial values. Ξ_0 , n (left) and H_0 , Ω_M (right) are fixed to their fiducial values.

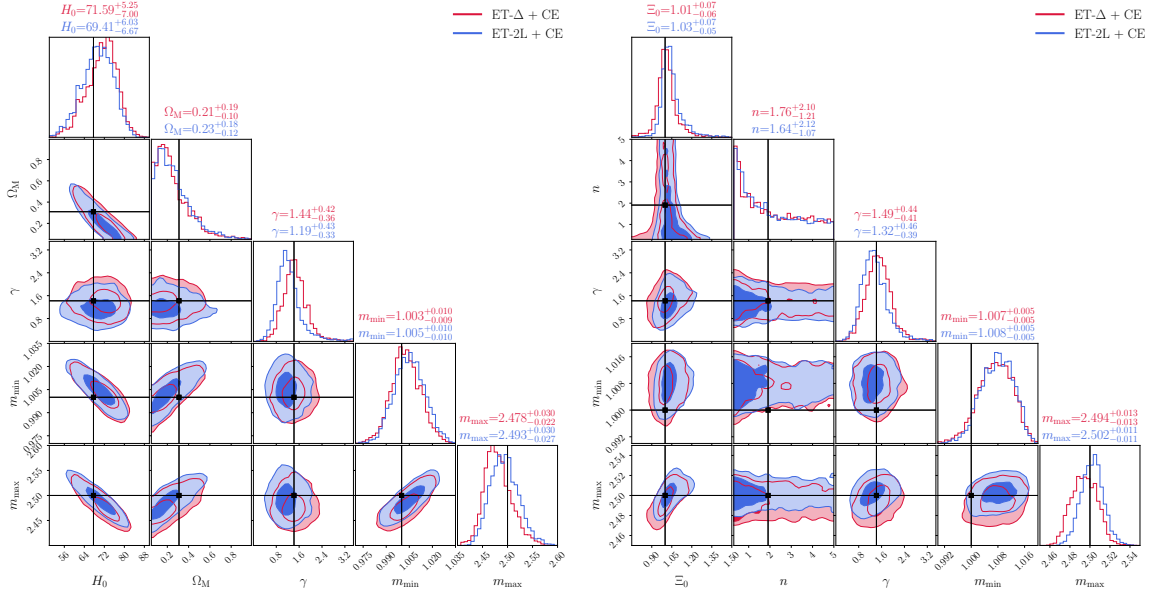


Figure 4. Posterior distribution of the parameters shown at the bottom for the ET- Δ +CE and ET-2L+CE network configurations. Contour shades represent, from dark to light, 1σ and 2σ credible regions. The black lines refer to the fiducial values. Ξ_0 , n (left) and H_0 , Ω_M (right) are fixed to their fiducial values.

5 Discussion

Our results provide forecasts on the precision that can be expected from a small subset of BNSs, corresponding to the events with $\text{SNR} > 50$, and therefore constitute only a lower bound on 3G capabilities. Indeed, for ET alone in the triangle (resp. 2L) configuration the selection criteria imposed in this study results in using 1.8% (resp. 2.2%) of the events that pass the less stringent detection criterion $\text{SNR} > 12$; for ET- Δ +CE (resp. ET-2L+CE) this fraction becomes 2.8% (resp. 3.2%). Even if their SNR is lower, we expect that the contribution of the events that have not been included can be significant, because of their large number compared to those that we have retained; furthermore, some of these events will be at higher redshift, where the effect of modified GW propagation is more important. Assuming a scaling of the relative precision with the number of events approximately as $1/\sqrt{N}$ (which can result from the fact that the events that we have not included have lower SNR but in general larger redshift and therefore better sensitivity to Ξ_0 , as discussed above), we expect that a percent level accuracy on Ξ_0 could be reached.

Given the importance of events at high redshifts for modified GW propagation, another very interesting perspective would be to perform a similar study with BBHs, which are detectable at higher redshifts. Recent work has explored their potential as dark sirens to constrain the expansion history [34, 98, 99]. In particular, there is consensus that, assuming a Λ CDM expansion history, BBHs as dark sirens provide their best constraint on $H(z)$ at intermediate redshifts rather than on H_0 and $\Omega_{m,0}$ taken individually [21, 32, 99, 100]. Specifically, for 3G detectors, ref. [99] forecasts a 2.4% precision on $H(z)$ at $z \sim 1.5$ using ~ 12000 events at $\text{SNR} > 60$. For comparison, our constraints on the Λ CDM expansion history correspond to a best constraint of 10% (6%) at $z \sim 0.23$ ($z \sim 0.28$) for the ET- Δ (2L) configuration when ET is alone, and a best constraint of 4% (3%) at $z \sim 0.37$ ($z \sim 0.38$) for the ET- Δ (2L) configuration in combination with CE, as illustrated by figure 5. These optimal redshifts are lower than the corresponding optimal redshift $z \sim 1.5$ for BBHs [99], as a consequence of the lower SNR of BNSs. This suggests that the two samples can be combined to obtain a more precise joint measurement which takes advantage of both. For Ξ_0 , on the other hand, there is no equivalent of the redshift that minimizes the relative uncertainty on deviations from GR. This is a consequence of the fact that the effect of modifications of gravity cumulates during propagation, in such a way that the parameter Ξ_0 encodes by design the maximum information that can be extracted from the data. In any case, eventually the optimal approach would be to work with a full CBC population to break degeneracies between the mass spectrum and the redshift distribution of the sources with a single hierarchical analysis [22, 34]. A crucial advantage of using BNSs, in particular, is that the BNS mass spectrum is restricted to a much narrower range, making its use less sensitive to the presence of putative peaks, changes in slope, and other features that can be prone to significant modeling systematics (see e.g. [101]); it is also expected to be more stable in redshift [102].

Finally, an interesting extension of this work would be to jointly use the spectral and galaxy catalog methods. Indeed our BNS catalog covers $z < 0.8$ which will be well-probed by upcoming galaxy surveys, such as Euclid [103] and LSST [104]. However, the galaxy catalog method, especially at the redshifts that can be reached by 3G detectors, must tackle delicate issues of catalog completeness (see [17, 25, 105] for recent discussions). At the current level of knowledge, we preferred here not to mix methods or simultaneously combine different sets of assumptions and instead study first their individual constraining power.

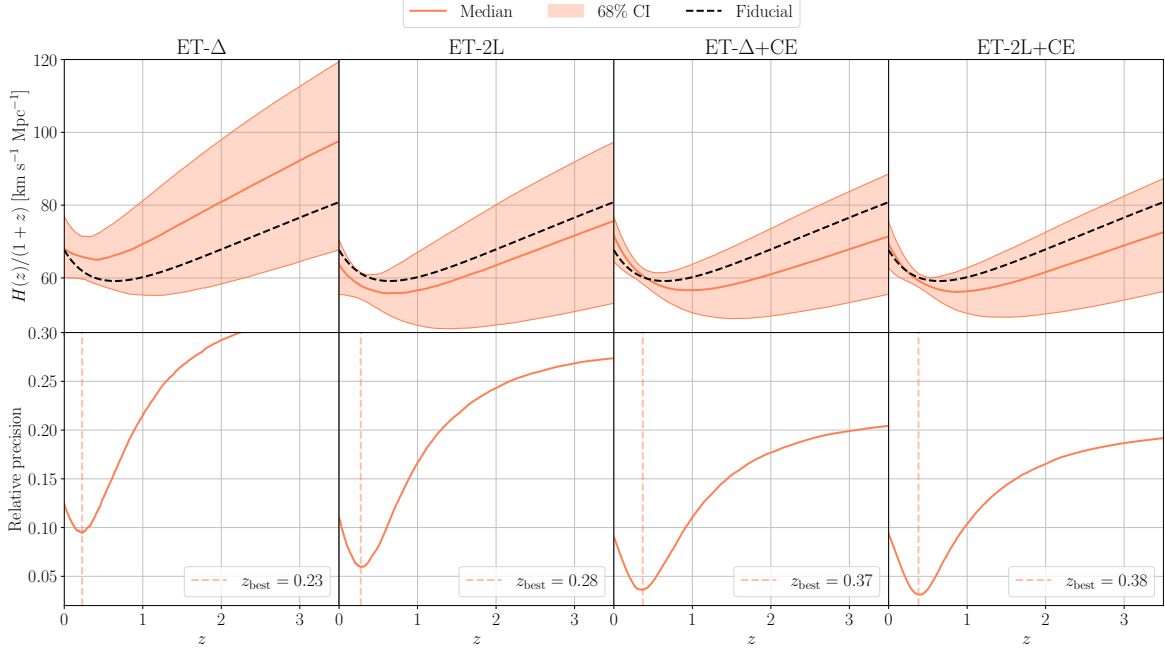


Figure 5. Constraints on the Hubble parameter $H(z)$ (top row) and its relative precision as defined in footnote 4 as a function of redshift (bottom row), for the configurations labeled at the top of each column. In the top row panels the shaded regions refer to the 68% c.l., while the solid-orange (dotted-black) line labels the median (fiducial) curve.

Acknowledgments. We thank Francesco Iacovelli, Andrea Iannicari, Davide Perrone, Davide Piras for useful discussions. This work is partially supported by the Spanish MCIN/AEI/10.13039/501100011033 under the Grants No. PID2020-113701GB-I00, PID2023-146517NB-I00 and CEX2024-001441-S, some of which include ERDF funds from the European Union, and by the MICINN with funding from the European Union NextGenerationEU (PRTR-C17.I1) and by the Generalitat de Catalunya. IFAE is partially funded by the CERCA program of the Generalitat de Catalunya. This project has received funding from the European Union’s Horizon Europe research and innovation programme under the Marie Skłodowska-Curie grant agreement No. 10181337. The research of M. Mag. and N.M. is supported by the SwissMap National Center for Competence in Research. The research of M. Mag. is supported by the SNSF grant CRSII5_213497. The work of M. Man. received support from the French government under the France 2030 investment plan, as part of the Initiative d’Excellence d’Aix-Marseille Université – A*MIDEX AMX-22-CEI-02. Computations made use of the Baobab cluster at the University of Geneva.

Appendix A: Dependence of the choice of n priors

As discussed in section 2, there is a degeneracy between the modified gravity parameters Ξ_0 and n for GR. Indeed, figure 6 illustrates that, when setting a wide priors, GR is compatible either with $\Xi_0 = 1$ for an arbitrary n or $n = 0$ for an arbitrary Ξ_0 . We assess how the choice of n_{\min} affects the marginal posterior distributions with the aim of identifying a physically motivated compromise to break this degeneracy. Setting $n_{\min} = 0.3$ allows us to exclude

the long tails in the Ξ_0 posterior, compatible with $n = 0$, without narrowing our prior unnecessarily.

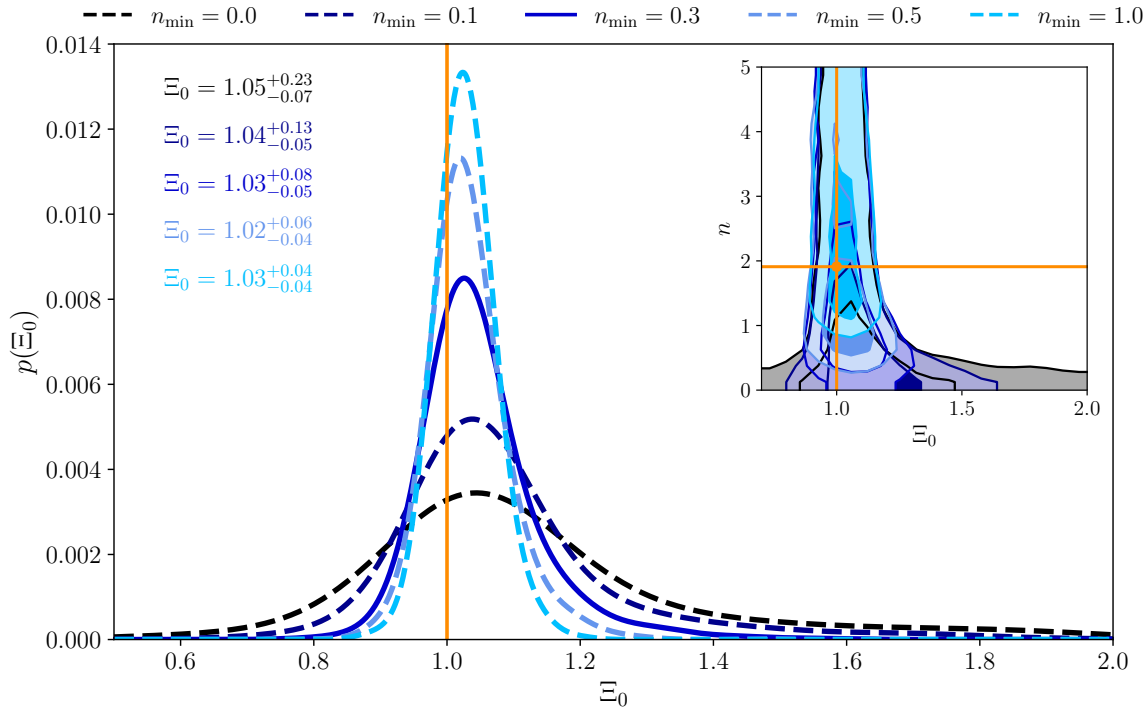


Figure 6. Marginalized posteriors $p(\Xi_0)$ for different choices of the lower prior bound n_{\min} . Increasing n_{\min} removes support at low n , tightening the distribution and shifting Ξ_0 toward $\simeq 1$. The inset shows the joint $p(\Xi_0, n)$ posterior, highlighting the parameter degeneracy and how truncating the prior in n projects onto a narrower, shifted constraint on Ξ_0 . The orange line and the blue solid line refer to the fiducial value and the final choice adopted in this study. Contour shades in the joint posterior distribution represent, from dark to light, 1σ and 2σ credible regions. H_0 and Ω_M are fixed to their fiducial values, and the marginalization is performed over the remaining hyper-parameters.

References

- [1] B. F. Schutz, “Determining the Hubble Constant from Gravitational Wave Observations,” *Nature* **323** (1986) 310–311.
- [2] D. F. Chernoff and L. S. Finn, “Gravitational radiation, inspiraling binaries, and cosmology,” *Astrophys. J. Lett.* **411** (1993) L5–L8, [arXiv:gr-qc/9304020](#).
- [3] D. E. Holz and S. A. Hughes, “Using gravitational-wave standard sirens,” *Astrophys. J.* **629** (2005) 15–22, [arXiv:astro-ph/0504616](#) [[astro-ph](#)].
- [4] N. Dalal, D. E. Holz, S. A. Hughes, and B. Jain, “Short GRB and binary black hole standard sirens as a probe of dark energy,” *Phys. Rev.* **D74** (2006) 063006, [arXiv:astro-ph/0601275](#) [[astro-ph](#)].
- [5] C. L. MacLeod and C. J. Hogan, “Precision of Hubble constant derived using black hole binary absolute distances and statistical redshift information,” *Phys. Rev.* **D77** (2008) 043512, [arXiv:0712.0618](#) [[astro-ph](#)].

- [6] S. Nissanke, D. E. Holz, S. Hughes, N. Dalal, and J. L. Sievers, “Exploring short gamma-ray bursts as gravitational-wave standard sirens,” *Astrophys. J.* **725** (2010) 496–514, [arXiv:0904.1017 \[astro-ph.CO\]](#).
- [7] C. Cutler and D. E. Holz, “Ultra-high precision cosmology from gravitational waves,” *Phys. Rev.* **D80** (2009) 104009, [arXiv:0906.3752 \[astro-ph.CO\]](#).
- [8] W. Del Pozzo, “Inference of the cosmological parameters from gravitational waves: application to second generation interferometers,” *Phys. Rev. D* **86** (2012) 043011, [arXiv:1108.1317 \[astro-ph.CO\]](#).
- [9] S. R. Taylor, J. R. Gair, and I. Mandel, “Hubble without the Hubble: Cosmology using advanced gravitational-wave detectors alone,” *Phys. Rev.* **D85** (2012) 023535, [arXiv:1108.5161 \[gr-qc\]](#).
- [10] S. R. Taylor and J. R. Gair, “Cosmology with the lights off: standard sirens in the Einstein Telescope era,” *Phys. Rev.* **D86** (2012) 023502, [arXiv:1204.6739 \[astro-ph.CO\]](#).
- [11] H.-Y. Chen, M. Fishbach, and D. E. Holz, “A two per cent Hubble constant measurement from standard sirens within five years,” *Nature* **562** (2018) 545, [arXiv:1712.06531 \[astro-ph.CO\]](#).
- [12] S. M. Feeney, H. V. Peiris, A. R. Williamson, S. M. Nissanke, D. J. Mortlock, J. Alsing, and D. Scolnic, “Prospects for resolving the Hubble constant tension with standard sirens,” *Phys. Rev. Lett.* **122** no. 6, (2019) 061105, [arXiv:1802.03404 \[astro-ph.CO\]](#).
- [13] R. Gray *et al.*, “Cosmological Inference using Gravitational Wave Standard Sirens: A Mock Data Challenge,” *Phys. Rev. D* **101** (2020) 122001, [arXiv:1908.06050 \[gr-qc\]](#).
- [14] S. Mukherjee, B. D. Wandelt, S. M. Nissanke, and A. Silvestri, “Accurate precision Cosmology with redshift unknown gravitational wave sources,” *Phys. Rev. D* **103** no. 4, (2021) 043520, [arXiv:2007.02943 \[astro-ph.CO\]](#).
- [15] S. Mastrogiovanni, L. Haegel, C. Karathanasis, I. Magana-Hernandez, and D. Steer, “Gravitational wave friction in light of GW170817 and GW190521,” *JCAP* **02** (10, 2021) 043, [arXiv:2010.04047 \[gr-qc\]](#).
- [16] S. Mukherjee, B. D. Wandelt, and J. Silk, “Testing the general theory of relativity using gravitational wave propagation from dark standard sirens,” *Mon. Not. Roy. Astron. Soc.* **502** no. 1, (2021) 1136–1144, [arXiv:2012.15316 \[astro-ph.CO\]](#).
- [17] A. Finke, S. Foffa, F. Iacovelli, M. Maggiore, and M. Mancarella, “Cosmology with LIGO/Virgo dark sirens: Hubble parameter and modified gravitational wave propagation,” *JCAP* **08** (2021) 026, [arXiv:2101.12660 \[astro-ph.CO\]](#).
- [18] A. Finke, S. Foffa, F. Iacovelli, M. Maggiore, and M. Mancarella, “Probing modified gravitational wave propagation with strongly lensed coalescing binaries,” *Phys. Rev. D* **104** no. 8, (2021) 084057, [arXiv:2107.05046 \[gr-qc\]](#).
- [19] A. Finke, S. Foffa, F. Iacovelli, M. Maggiore, and M. Mancarella, “Modified gravitational wave propagation and the binary neutron star mass function,” *Phys. Dark Univ.* **36** (2022) 100994, [arXiv:2108.04065 \[gr-qc\]](#).
- [20] A. Palmese, C. R. Bom, S. Mucesh, and W. G. Hartley, “A Standard Siren Measurement of the Hubble Constant Using Gravitational-wave Events from the First Three LIGO/Virgo Observing Runs and the DESI Legacy Survey,” *Astrophys. J.* **943** no. 1, (2023) 56, [arXiv:2111.06445 \[astro-ph.CO\]](#).
- [21] M. Mancarella, E. Genoud-Prachex, and M. Maggiore, “Cosmology and modified gravitational wave propagation from binary black hole population models,” *Phys. Rev. D* **105** no. 6, (2022) 064030, [arXiv:2112.05728 \[gr-qc\]](#).

- [22] J. M. Ezquiaga and D. E. Holz, “Spectral Sirens: Cosmology from the Full Mass Distribution of Compact Binaries,” *Phys. Rev. Lett.* **129** no. 6, (2022) 061102, [arXiv:2202.08240 \[astro-ph.CO\]](#).
- [23] K. Leyde, S. Mastrogiovanni, D. A. Steer, E. Chassande-Mottin, and C. Karathanasis, “Current and future constraints on cosmology and modified gravitational wave friction from binary black holes,” *JCAP* **09** (2022) 012, [arXiv:2202.00025 \[gr-qc\]](#).
- [24] S. Mukherjee, A. Krolewski, B. D. Wandelt, and J. Silk, “Cross-correlating dark sirens and galaxies: measurement of H_0 from GWTC-3 of LIGO-Virgo-KAGRA,” [arXiv:2203.03643 \[astro-ph.CO\]](#).
- [25] N. Borghi, M. Mancarella, M. Moresco, M. Tagliazucchi, F. Iacovelli, A. Cimatti, and M. Maggiore, “Cosmology and Astrophysics with Standard Sirens and Galaxy Catalogs in View of Future Gravitational Wave Observations,” *Astrophys. J.* **964** no. 2, (2024) 191, [arXiv:2312.05302 \[astro-ph.CO\]](#).
- [26] J. Ferri, I. L. Tashiro, L. R. Abramo, I. Matos, M. Quartin, and R. Sturani, “A robust cosmic standard ruler from the cross-correlations of galaxies and dark sirens,” *JCAP* **04** (2025) 008, [arXiv:2412.00202 \[astro-ph.CO\]](#).
- [27] B. P. Abbott *et al.*, “GW170817: Observation of Gravitational Waves from a Binary Neutron Star Inspiral,” *Phys. Rev. Lett.* **119** no. 16, (2017) 161101, [arXiv:1710.05832 \[gr-qc\]](#).
- [28] **LIGO Scientific, Virgo, Fermi-GBM, INTEGRAL** Collaboration, B. P. Abbott *et al.*, “Gravitational Waves and Gamma-rays from a Binary Neutron Star Merger: GW170817 and GRB 170817A,” *Astrophys. J. Lett.* **848** no. 2, (2017) L13, [arXiv:1710.05834 \[astro-ph.HE\]](#).
- [29] R. Gray, C. Messenger, and J. Veitch, “A pixelated approach to galaxy catalogue incompleteness: improving the dark siren measurement of the Hubble constant,” *Mon. Not. Roy. Astron. Soc.* **512** no. 1, (2022) 1127–1140, [arXiv:2111.04629 \[astro-ph.CO\]](#).
- [30] J. R. Gair *et al.*, “The Hitchhiker’s guide to the galaxy catalog approach for gravitational wave cosmology,” [arXiv:2212.08694 \[gr-qc\]](#).
- [31] S. Mastrogiovanni, G. Pierra, S. Perriès, D. Laghi, G. Caneva Santoro, A. Ghosh, R. Gray, C. Karathanasis, and K. Leyde, “ICAROGW: A python package for inference of astrophysical population properties of noisy, heterogeneous, and incomplete observations,” *Astron. Astrophys.* **682** (2024) A167, [arXiv:2305.17973 \[astro-ph.CO\]](#).
- [32] W. M. Farr, M. Fishbach, J. Ye, and D. Holz, “A Future Percent-Level Measurement of the Hubble Expansion at Redshift 0.8 With Advanced LIGO,” *Astrophys. J. Lett.* **883** no. 2, (2019) L42, [arXiv:1908.09084 \[astro-ph.CO\]](#).
- [33] S. Mastrogiovanni, K. Leyde, C. Karathanasis, E. Chassande-Mottin, D. A. Steer, J. Gair, A. Ghosh, R. Gray, S. Mukherjee, and S. Rinaldi, “On the importance of source population models for gravitational-wave cosmology,” *Phys. Rev. D* **104** no. 6, (2021) 062009, [arXiv:2103.14663 \[gr-qc\]](#).
- [34] H.-Y. Chen, J. M. Ezquiaga, and I. Gupta, “Cosmography with next-generation gravitational wave detectors,” *Class. Quant. Grav.* **41** no. 12, (2024) 125004, [arXiv:2402.03120 \[gr-qc\]](#).
- [35] G. Pierra and A. Papadopoulos, “Heavy Black-Holes Also Matter in Standard Siren Cosmology,” [arXiv:2601.03257 \[astro-ph.CO\]](#).
- [36] M. Tagliazucchi, M. Moresco, N. Borghi, and C. Ciapetti, “Mind the peak: improving cosmological constraints from GWTC-4.0 spectral sirens using semiparametric mass models,” [arXiv:2601.03347 \[astro-ph.CO\]](#).
- [37] A. Palmese and S. Mastrogiovanni, “Gravitational Wave Cosmology,” [arXiv:2502.00239 \[astro-ph.CO\]](#).

- [38] G. Pierra and S. Mastrogiovanni, “Gravitational wave cosmology : an introduction,” [arXiv:2507.10597 \[gr-qc\]](#).
- [39] C. Messenger and J. Read, “Measuring a cosmological distance-redshift relationship using only gravitational wave observations of binary neutron star coalescences,” *Phys. Rev. Lett.* **108** (2012) 091101, [arXiv:1107.5725 \[gr-qc\]](#).
- [40] M. Punturo *et al.*, “The Einstein Telescope: A third-generation gravitational wave observatory,” *Class. Quant. Grav.* **27** (2010) 194002.
- [41] S. Hild *et al.*, “Sensitivity Studies for Third-Generation Gravitational Wave Observatories,” *Class. Quant. Grav.* **28** (2011) 094013, [arXiv:1012.0908 \[gr-qc\]](#).
- [42] M. Maggiore *et al.*, “Science Case for the Einstein Telescope,” *JCAP* **2020** no. 03, (2020) 050, [arXiv:1912.02622 \[astro-ph.CO\]](#).
- [43] D. Reitze *et al.*, “Cosmic Explorer: The U.S. Contribution to Gravitational-Wave Astronomy beyond LIGO,” *Bull. Am. Astron. Soc.* **51** no. 7, (2019) 035, [arXiv:1907.04833 \[astro-ph.IM\]](#).
- [44] M. Evans *et al.*, “A Horizon Study for Cosmic Explorer: Science, Observatories, and Community,” (9, 2021) , [arXiv:2109.09882 \[astro-ph.IM\]](#).
- [45] M. Evans *et al.*, “Cosmic Explorer: A Submission to the NSF MPSAC ngGW Subcommittee,” (6, 2023) , [arXiv:2306.13745 \[astro-ph.IM\]](#).
- [46] M. Branchesi *et al.*, “Science with the Einstein Telescope: a comparison of different designs,” *JCAP* **2023** no. 07, (2023) 068, [arXiv:2303.15923 \[gr-qc\]](#).
- [47] **ET** Collaboration, A. Abac *et al.*, “The Science of the Einstein Telescope,” [arXiv:2503.12263 \[gr-qc\]](#).
- [48] S. Borhanian, A. Dhani, A. Gupta, K. G. Arun, and B. S. Sathyaprakash, “Dark Sirens to Resolve the Hubble–Lemaître Tension,” *Astrophys. J. Lett.* **905** no. 2, (2020) L28, [arXiv:2007.02883 \[astro-ph.CO\]](#).
- [49] N. Muttoni, D. Laghi, N. Tamanini, S. Marsat, and D. Izquierdo-Villalba, “Dark siren cosmology with binary black holes in the era of third-generation gravitational wave detectors,” *Phys. Rev. D* **108** no. 4, (2023) 043543, [arXiv:2303.10693 \[astro-ph.CO\]](#).
- [50] M. Moresco *et al.*, “Unveiling the Universe with emerging cosmological probes,” *Living Rev. Rel.* **25** no. 1, (2022) 6, [arXiv:2201.07241 \[astro-ph.CO\]](#).
- [51] S. Mastrogiovanni, D. Laghi, R. Gray, G. C. Santoro, A. Ghosh, C. Karathanasis, K. Leyde, D. A. Steer, S. Perries, and G. Pierra, “Joint population and cosmological properties inference with gravitational waves standard sirens and galaxy surveys,” *Phys. Rev. D* **108** no. 4, (2023) 042002, [arXiv:2305.10488 \[astro-ph.CO\]](#).
- [52] R. Gray *et al.*, “Joint cosmological and gravitational-wave population inference using dark sirens and galaxy catalogues,” *JCAP* **12** (2023) 023, [arXiv:2308.02281 \[astro-ph.CO\]](#).
- [53] I. D. Saltas, I. Sawicki, L. Amendola, and M. Kunz, “Anisotropic Stress as a Signature of Nonstandard Propagation of Gravitational Waves,” *Phys. Rev. Lett.* **113** (2014) 191101, [arXiv:1406.7139 \[astro-ph.CO\]](#).
- [54] L. Lombriser and A. Taylor, “Breaking a Dark Degeneracy with Gravitational Waves,” *JCAP* **1603** (2016) 031, [arXiv:1509.08458 \[astro-ph.CO\]](#).
- [55] A. Nishizawa, “Generalized framework for testing gravity with gravitational-wave propagation. I. Formulation,” *Phys. Rev.* **D97** (2018) 104037, [arXiv:1710.04825 \[gr-qc\]](#).
- [56] S. Arai and A. Nishizawa, “Generalized framework for testing gravity with gravitational-wave propagation. II. Constraints on Horndeski theory,” *Phys. Rev. D* **97** no. 10, (2018) 104038, [arXiv:1711.03776 \[gr-qc\]](#).

- [57] E. Belgacem, Y. Dirian, S. Foffa, and M. Maggiore, “The gravitational-wave luminosity distance in modified gravity theories,” *Phys. Rev.* **D97** (2018) 104066, [arXiv:1712.08108 \[astro-ph.CO\]](#).
- [58] L. Amendola, I. Sawicki, M. Kunz, and I. D. Saltas, “Direct detection of gravitational waves can measure the time variation of the Planck mass,” *JCAP* **08** (2018) 030, [arXiv:1712.08623 \[astro-ph.CO\]](#).
- [59] E. Belgacem, Y. Dirian, S. Foffa, and M. Maggiore, “Modified gravitational-wave propagation and standard sirens,” *Phys. Rev.* **D98** (2018) 023510, [arXiv:1805.08731 \[gr-qc\]](#).
- [60] A. Nishizawa and S. Arai, “Generalized framework for testing gravity with gravitational-wave propagation. III. Future prospect,” *Phys. Rev. D* **99** no. 10, (2019) 104038, [arXiv:1901.08249 \[gr-qc\]](#).
- [61] E. Belgacem, Y. Dirian, A. Finke, S. Foffa, and M. Maggiore, “Nonlocal gravity and gravitational-wave observations,” *JCAP* **11** (2019) 022, [arXiv:1907.02047 \[astro-ph.CO\]](#).
- [62] E. Belgacem, Y. Dirian, A. Finke, S. Foffa, and M. Maggiore, “Gravity in the infrared and effective nonlocal models,” *JCAP* **04** (2020) 010, [arXiv:2001.07619 \[astro-ph.CO\]](#).
- [63] **LISA Cosmology Working Group** Collaboration, E. Belgacem *et al.*, “Testing modified gravity at cosmological distances with LISA standard sirens,” *JCAP* **07** (2019) 024, [arXiv:1906.01593 \[astro-ph.CO\]](#).
- [64] E. Belgacem, S. Foffa, M. Maggiore, and T. Yang, “Gaussian processes reconstruction of modified gravitational wave propagation,” *Phys. Rev. D* **101** no. 6, (2020) 063505, [arXiv:1911.11497 \[astro-ph.CO\]](#).
- [65] A. A. Starobinsky, “Disappearing cosmological constant in f(R) gravity,” *JETP Lett.* **86** (2007) 157–163, [arXiv:0706.2041 \[astro-ph\]](#).
- [66] W. Hu and I. Sawicki, “Models of f(R) Cosmic Acceleration that Evade Solar-System Tests,” *Phys. Rev. D* **76** (2007) 064004, [arXiv:0705.1158 \[astro-ph\]](#).
- [67] C. Brans and R. H. Dicke, “Mach’s principle and a relativistic theory of gravitation,” *Phys. Rev.* **124** (1961) 925–935.
- [68] A. Nicolis, R. Rattazzi, and E. Trincherini, “The Galileon as a local modification of gravity,” *Phys. Rev. D* **79** (2009) 064036, [arXiv:0811.2197 \[hep-th\]](#).
- [69] N. Chow and J. Khoury, “Galileon Cosmology,” *Phys. Rev. D* **80** (2009) 024037, [arXiv:0905.1325 \[hep-th\]](#).
- [70] M. Maggiore, “Phantom dark energy from nonlocal infrared modifications of general relativity,” *Phys.Rev.* **D89** (2014) 043008, [arXiv:1307.3898 \[hep-th\]](#).
- [71] M. Maggiore and M. Mancarella, “Nonlocal gravity and dark energy,” *Phys. Rev. D* **90** no. 2, (2014) 023005, [arXiv:1402.0448 \[hep-th\]](#).
- [72] **LIGO Scientific, VIRGO, KAGRA** Collaboration, A. G. Abac *et al.*, “GWTC-4.0: Constraints on the Cosmic Expansion Rate and Modified Gravitational-wave Propagation,” [arXiv:2509.04348 \[astro-ph.CO\]](#).
- [73] **LIGO Scientific, KAGRA, VIRGO** Collaboration, A. G. Abac *et al.*, “GWTC-4.0: An Introduction to Version 4.0 of the Gravitational-Wave Transient Catalog,” *Astrophys. J. Lett.* **995** no. 1, (2025) L18, [arXiv:2508.18080 \[gr-qc\]](#).
- [74] **LIGO Scientific, VIRGO, KAGRA** Collaboration, A. G. Abac *et al.*, “GWTC-4.0: Updating the Gravitational-Wave Transient Catalog with Observations from the First Part of the Fourth LIGO-Virgo-KAGRA Observing Run,” [arXiv:2508.18082 \[gr-qc\]](#).

- [75] **LIGO Scientific, Virgo** Collaboration, R. Abbott *et al.*, “GWTC-2: Compact Binary Coalescences Observed by LIGO and Virgo During the First Half of the Third Observing Run,” *Phys. Rev. X* **11** (2021) 021053, [arXiv:2010.14527 \[gr-qc\]](#).
- [76] **LIGO Scientific, VIRGO** Collaboration, R. Abbott *et al.*, “GWTC-2.1: Deep extended catalog of compact binary coalescences observed by LIGO and Virgo during the first half of the third observing run,” *Phys. Rev. D* **109** no. 2, (2024) 022001, [arXiv:2108.01045 \[gr-qc\]](#).
- [77] **KAGRA, VIRGO, LIGO Scientific** Collaboration, R. Abbott *et al.*, “GWTC-3: Compact Binary Coalescences Observed by LIGO and Virgo during the Second Part of the Third Observing Run,” *Phys. Rev. X* **13** no. 4, (2023) 041039, [arXiv:2111.03606 \[gr-qc\]](#).
- [78] A. Chen, R. Gray, and T. Baker, “Testing the nature of gravitational wave propagation using dark sirens and galaxy catalogues,” *JCAP* **02** (2024) 035, [arXiv:2309.03833 \[gr-qc\]](#).
- [79] T. J. Loredo, “Accounting for source uncertainties in analyses of astronomical survey data,” *AIP Conf. Proc.* **735** (2004) 195, [arXiv:astro-ph/0409387](#).
- [80] M. R. Adams, N. J. Cornish, and T. B. Littenberg, “Astrophysical Model Selection in Gravitational Wave Astronomy,” *Phys. Rev. D* **86** (2012) 124032, [arXiv:1209.6286 \[gr-qc\]](#).
- [81] I. Mandel, W. M. Farr, and J. R. Gair, “Extracting distribution parameters from multiple uncertain observations with selection biases,” *Mon. Not. Roy. Astron. Soc.* **486** (2019) 1086–1093, [arXiv:1809.02063 \[physics.data-an\]](#).
- [82] E. Thrane and C. Talbot, “An introduction to Bayesian inference in gravitational-wave astronomy: parameter estimation, model selection, and hierarchical models,” *Publ. Astron. Soc. Austral.* **36** (2019) e010, [arXiv:1809.02293 \[astro-ph.IM\]](#).
- [83] S. Vitale, D. Gerosa, W. M. Farr, and S. R. Taylor, “Inferring the properties of a population of compact binaries in presence of selection effects,” [arXiv:2007.05579 \[astro-ph.IM\]](#).
- [84] P. Madau and M. Dickinson, “Cosmic Star Formation History,” *Ann. Rev. Astron. Astrophys.* **52** (2014) 415–486, [arXiv:1403.0007 \[astro-ph.CO\]](#).
- [85] P. Madau and T. Fragos, “Radiation Backgrounds at Cosmic Dawn: X-Rays from Compact Binaries,” *Astrophys. J.* **840** (2017) 39, [arXiv:1606.07887 \[astro-ph.GA\]](#).
- [86] F. Iacovelli, M. Mancarella, S. Foffa, and M. Maggiore, “Forecasting the detection capabilities of third-generation gravitational-wave detectors using GWFIRST,” *Astrophys. J.* **941** no. 2, (2022) 208, [arXiv:2207.02771 \[gr-qc\]](#).
- [87] M. Mancarella, F. Iacovelli, S. Foffa, N. Muttoni, and M. Maggiore, “Accurate standard siren cosmology with joint gravitational-wave and γ -ray burst observations,” (5, 2024) , [arXiv:2405.02286 \[astro-ph.HE\]](#).
- [88] M. Chevallier and D. Polarski, “Accelerating universes with scaling dark matter,” *Int.J.Mod.Phys. D* **10** (2001) 213–224, [arXiv:gr-qc/0009008 \[gr-qc\]](#).
- [89] E. V. Linder, “Exploring the expansion history of the universe,” *Phys.Rev.Lett.* **90** (2003) 091301, [arXiv:astro-ph/0208512 \[astro-ph\]](#).
- [90] **H0DN** Collaboration, S. Casertano *et al.*, “The Local Distance Network: a community consensus report on the measurement of the Hubble constant at 1% precision,” [arXiv:2510.23823 \[astro-ph.CO\]](#).
- [91] Y.-S. Song, W. Hu, and I. Sawicki, “The Large Scale Structure of $f(R)$ Gravity,” *Phys. Rev. D* **75** (2007) 044004, [arXiv:astro-ph/0610532](#).
- [92] E. E. Flanagan, “The Sensitivity of the laser interferometer gravitational wave observatory (LIGO) to a stochastic background, and its dependence on the detector orientations,” *Phys. Rev. D* **48** (1993) 2389–2407, [arXiv:astro-ph/9305029](#).

- [93] N. Christensen, “Optimal detection strategies for measuring the stochastic gravitational radiation background with laser interferometric antennas,” *Phys. Rev. D* **55** (1997) 448–454.
- [94] **LIGO Scientific, VIRGO, KAGRA** Collaboration, A. G. Abac *et al.*, “GWTC-4.0: Population Properties of Merging Compact Binaries,” [arXiv:2508.18083](#) [[astro-ph.HE](#)].
- [95] S. Khan, S. Husa, M. Hannam, F. Ohme, M. Pürrer, X. Jiménez Forteza, and A. Bohé, “Frequency-domain gravitational waves from nonprecessing black-hole binaries. II. A phenomenological model for the advanced detector era,” *Phys. Rev. D* **93** (2016) 044007, [arXiv:1508.07253](#) [[gr-qc](#)].
- [96] F. Iacovelli, M. Mancarella, S. Foffa, and M. Maggiore, “GWFAST: a Fisher information matrix Python code for third-generation gravitational-wave detectors,” *Astrophys. J. Suppl.* **263** (2022) 2, [arXiv:2207.06910](#) [[astro-ph.IM](#)].
- [97] J. Buchner, “UltraNest – a robust, general purpose Bayesian inference engine,” [arXiv:2101.09604](#) [[stat.CO](#)].
- [98] M. Califano, I. De Martino, and D. Vernieri, “Joint estimation of the cosmological model and the mass and redshift distributions of the binary black hole population with the Einstein Telescope,” *Phys. Rev. D* **111** no. 12, (2025) 123535, [arXiv:2503.19061](#) [[astro-ph.CO](#)].
- [99] M. Tagliacuzzi, M. Moresco, A. Agapito, M. Mancarella, S. Ferraiuolo, S. Mastrogiovanni, N. Borghi, F. Pannarale, and D. Bonacorsi, “Pushing spectral siren cosmology into the third-generation era: a blinded mock data challenge,” [arXiv:2602.17756](#) [[astro-ph.CO](#)].
- [100] A. M. Farah, T. A. Callister, J. M. Ezquiaga, M. Zevin, and D. E. Holz, “No Need to Know: Toward Astrophysics-free Gravitational-wave Cosmology,” *Astrophys. J.* **978** no. 2, (2025) 153, [arXiv:2404.02210](#) [[astro-ph.CO](#)].
- [101] G. Pierra, S. Mastrogiovanni, S. Perriès, and M. Mapelli, “Study of systematics on the cosmological inference of the Hubble constant from gravitational wave standard sirens,” *Phys. Rev. D* **109** no. 8, (2024) 083504, [arXiv:2312.11627](#) [[astro-ph.CO](#)].
- [102] S. K. Roy, L. A. C. van Son, A. Ray, and W. M. Farr, “Cosmology with Binary Neutron Stars: Does Mass–Redshift Correlation Matter?,” *Astrophys. J. Lett.* **985** no. 2, (2025) L33, [arXiv:2411.02494](#) [[astro-ph.CO](#)].
- [103] **Euclid** Collaboration, R. Scaramella *et al.*, “Euclid preparation. I. The Euclid Wide Survey,” *Astron. Astrophys.* **662** (2022) A112, [arXiv:2108.01201](#) [[astro-ph.CO](#)].
- [104] **LSST** Collaboration, Z. Ivezić *et al.*, “LSST: from Science Drivers to Reference Design and Anticipated Data Products,” *Astrophys. J.* **873** no. 2, (2019) 111, [arXiv:0805.2366](#) [[astro-ph](#)].
- [105] C. Dalang, B. Fiorini, and T. Baker, “Large scale structure prior knowledge in the dark siren method,” [arXiv:2410.03275](#) [[astro-ph.CO](#)].